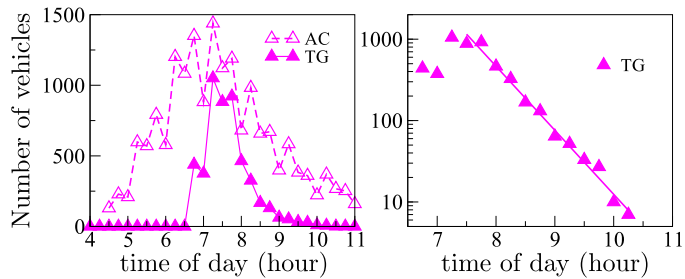


# Macroscopic dynamics and the collapse of urban traffic

Olmos et al. 10.1073/pnas.XXXXXXXXXX

## Supporting Information(SI)



**Fig. S1. Exponential decay in Bogotá.** Temporal profile of the vehicle trips in the road network during the morning peak hour. As in Bogotá the maximal travel demand occurs around 7:30, the target group (TG) corresponds to vehicles entering the network from 6:30 to 7:30. Empty symbols are for all travelers (AC) while the filled ones corresponds to the target group.

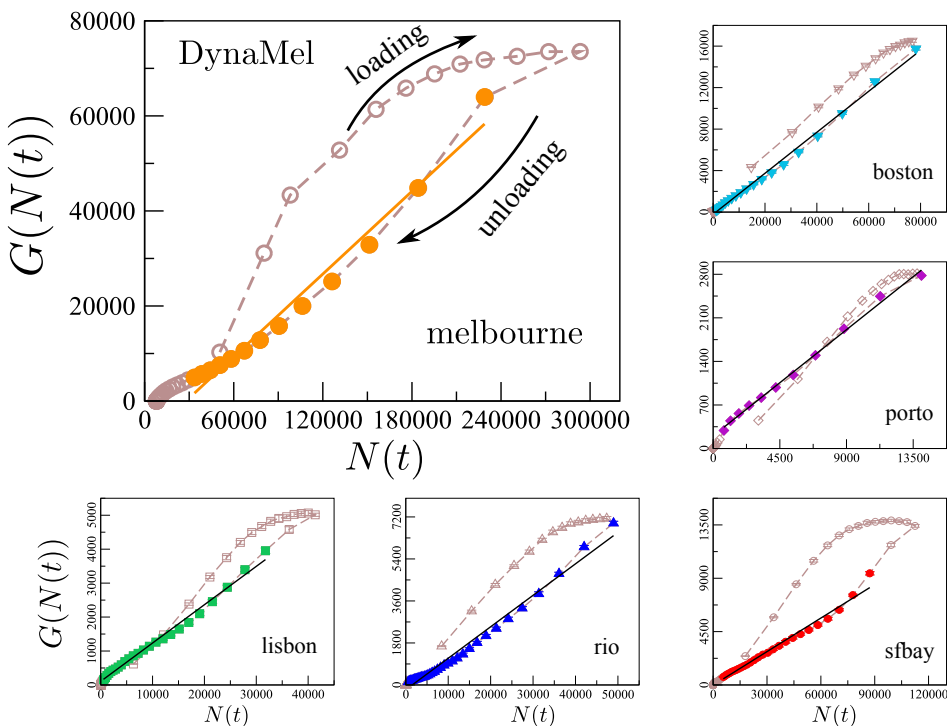


**Fig. S2. Exit function  $G(N(t))$  vs the number of vehicles of the target group still in the network  $N(t)$ .** From both models, DynaMel and the Cellular Automaton, a reasonably linear relationship (colored symbols) is obtained for the recovery period, i.e.  $G(N(t)) = |\frac{dN(t)}{dt}| \propto N(t)$  for  $t \geq t_o$ . The obtained hysteresis loops are larger than the usually observed for the total outflow of the network. That is a consequence of tracking the vehicles of the target group  $N(t)$ , where naturally there is an abrupt demand interruption at  $t_o$ .

Capacity $C_e$ [veh/h]	Prob. $p$
8100	1.00
6900	1.00
5400	1.00
1900	0.70370
950	0.35185

**Table S1.** To model the intersection dynamics, we have categorized the roads capacities in three levels. Motorways and primary roads (in the OSM classification) have a delivery probability  $p=1.0$ . Otherwise  $p$  is the ratio between the real road capacity  $C_e$  (taken from OSM) and the maximum capacity for a two-lanes secondary road that we set to 2700[veh/h]. The table shows the probabilities used based on the capacity  $C_e$  of the originating link  $e$ . In this way, we capture the hierarchical structure in the road networks.

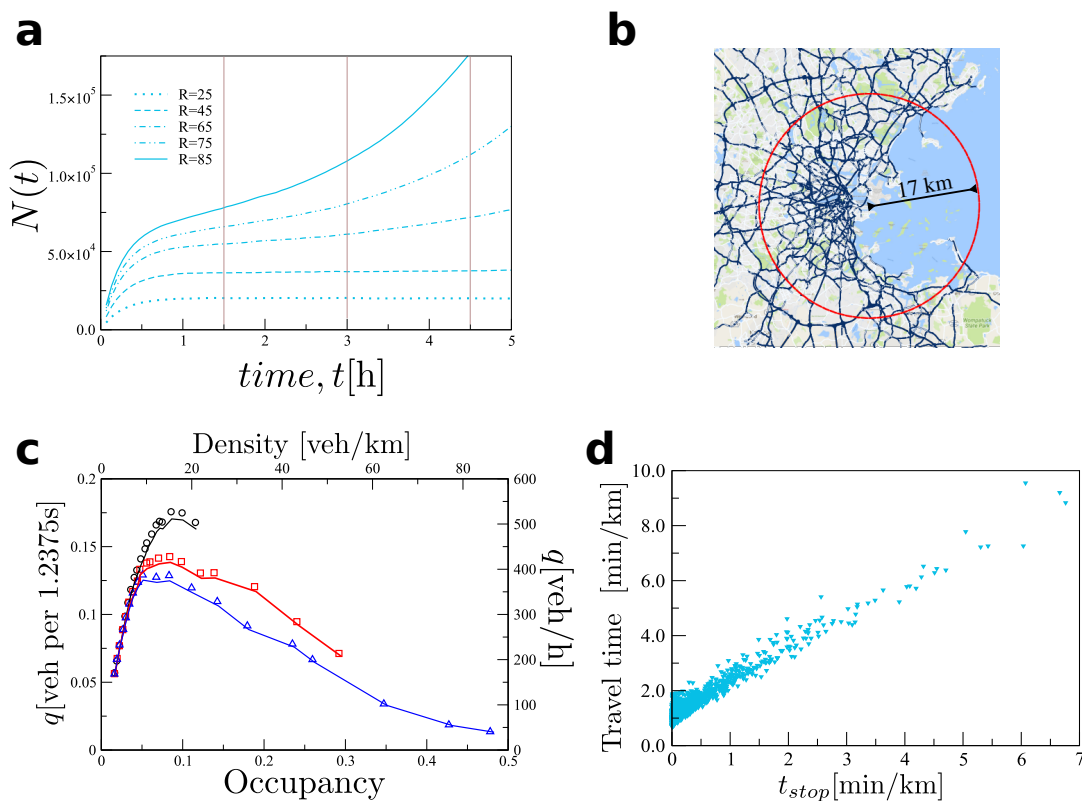


**Fig. S3. Model validation.** Despite the simplicity of the model, many generic features of the urban traffic were correctly reproduced. (a) Using Boston as case study, we load the road network with several constant insertion rate  $R$ . Here we show the temporal profile of the total number of cars in the system. (b) For each case we measured the average flow and density for the links inside the red circle, which the Boston business district where the distribution of congestion over space is more homogeneous. (c) We measure the Macroscopic Fundamental Diagram (MFD) after a transient period of half 1.5 (black), 2 (red) and 3 (blue) hours. We can observe how if the average vehicle density is higher than  $\approx 18$  veh/km, the average network flow drops as time passes (1, 2). (c) Under the same conditions of the previous figures, we observe a linear relationship between the trip time per unit distance and the stop time per unit distance, which is in agreement with empirical observations in (3, 4).

	City					
	Boston	Porto	Lisbon	Rio	SF Bay	Melbourne
Exponential	0.0236	0.0356	0.0256	0.0501068	0.0370	0.0440
Gamma	0.0830	0.0273	0.0260	0.0695	0.0507	0.0170
Weibull	0.0146	0.0235	0.0252	0.0179	0.0219	0.0166

**Table S2.** Kolmogorov-Smirnov test statistics for exponential, gamma and weibull distribution fits for the remaining travel time.

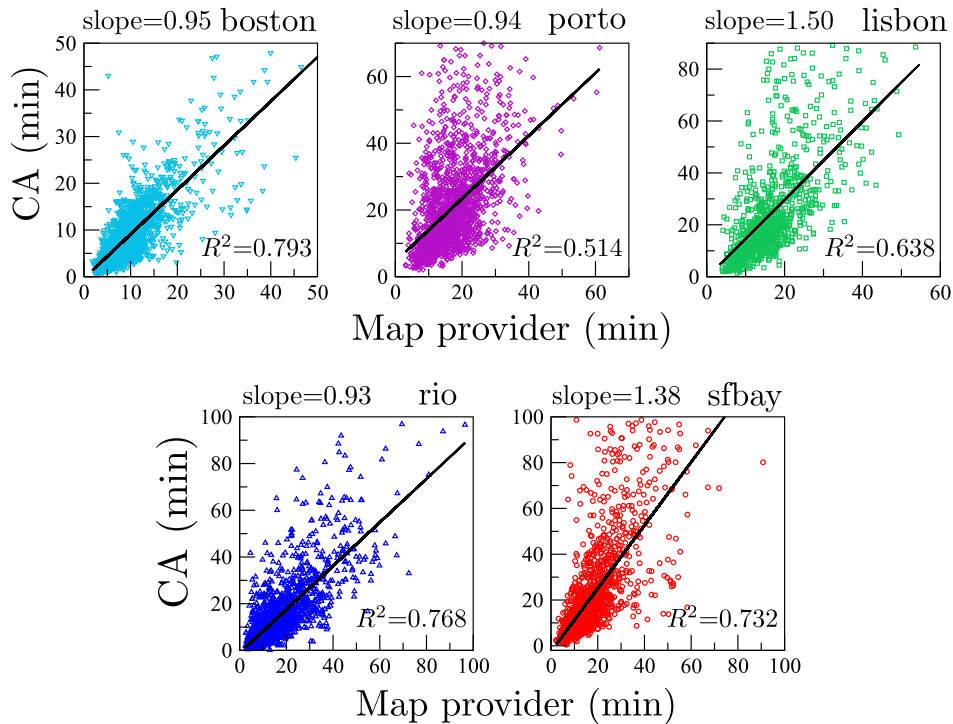


**Fig. S4.** Travel time comparisons Comparison of travel times between the CA simulations versus routes obtained from the Google API. OD samples consist of 2,000 OD pairs with the highest commuting flow magnitudes for each city. For each city, the volume demand corresponds to  $V_{ca}$  defined in the manuscript.

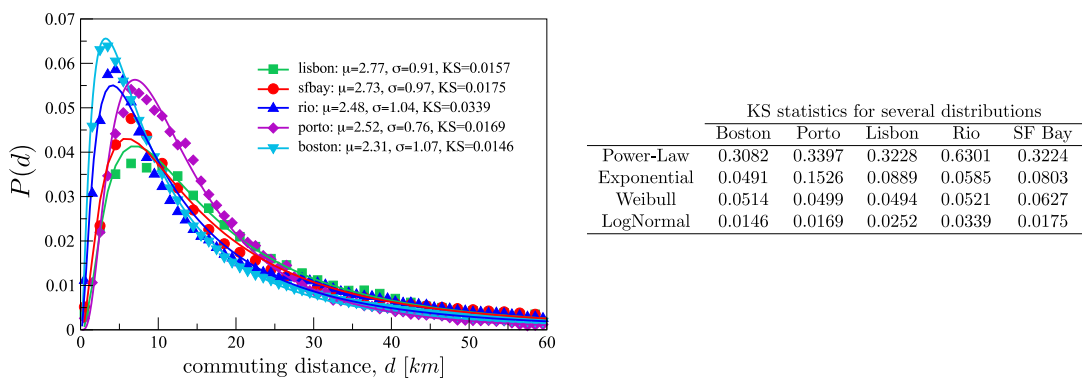


**Fig. S5.** Distribution of commuting distances,  $d$ [km], in the morning peak. All numerical results follow a lognormal distribution  $P(d; \mu, \sigma) = \frac{1}{\sqrt{2\pi}\sigma d_b} e^{-(\ln(d)-\mu)^2/2\sigma^2}$ . The distribution parameters and the Kolmogorov-Smirnov test are depicted in the legend.(Right) KS test statistics for power-law, exponential, weibull and lognormal distribution fits for the commuting distances.

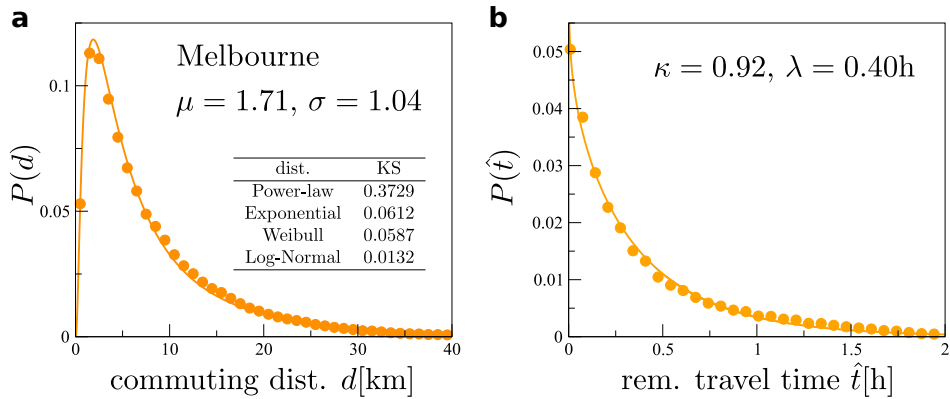


**Fig. S6. Commuting distances and remaining travel time for the case of Melbourne.** (a) Similar to the other five cities, the commuting distances,  $d$ , follow a log-normal distribution with the parameters depicted in the figure. Inset: The KS statistic for several distribution fits. (b) In the same way, the remaining travel time  $\hat{t}$  follows a weibull distribution.

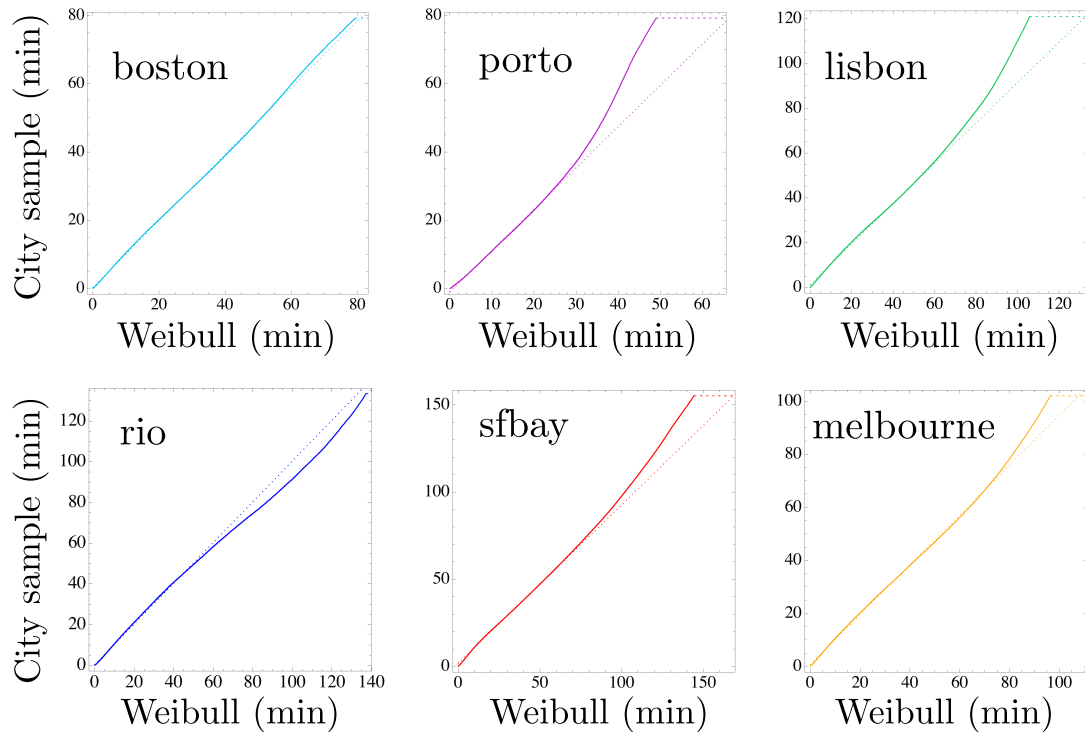


**Fig. S7. Q-Q plots for the Weibull distribution of the remaining travel times  $\hat{t}$ .** Outliers are evident at the high end of the range. Otherwise, the data fit the Weibull model well.

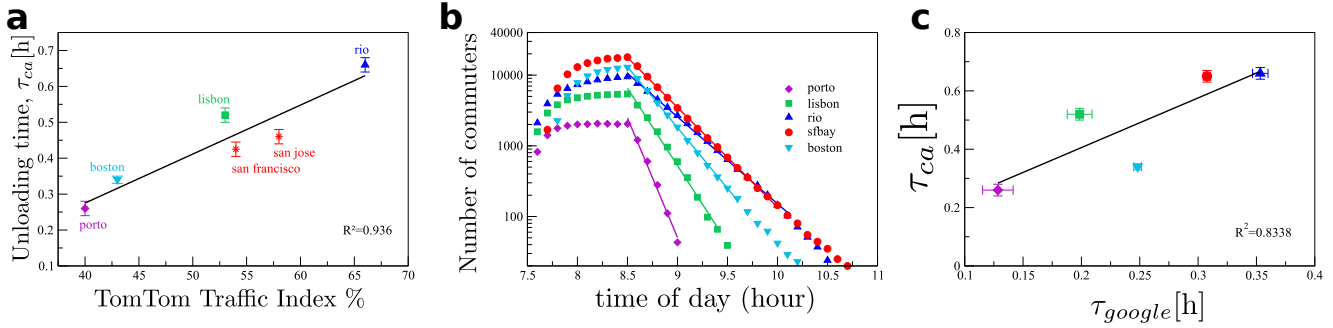


**Fig. S8. Comparison to TomTom Traffic Index and unloading time from GoogleAPI.** (a) TomTom is one of the major GPS navigation device companies. Based on speed measurements on individual road segments and entire networks, their traffic index is the estimate of the extra travel time per day due to congestion. It is obtained by computing the increase of the average travel times during peak hours compared with the free flow situation. As TomTom does not report the traffic index for Bay Area, we simulate the two cities separately, neglecting the inter-city trips. Remarkably, we find a very good linear relation between  $\tau$  and the TomTom Traffic Index for the morning peak hour reported in 2016. We try to measure the realistic unloading time using GoogleAPI. First we choose the 5% of trips from the total volume demand in the ODs. Then, we assign randomly for each trip the departure time over the peak hour (7:30 to 8:30 am) and then ask to GoogleAPI the travel time. With this information we reproduce the exponential unloading (b). (c) We compare the results from GoogleAPI with the TomTom traffic index.

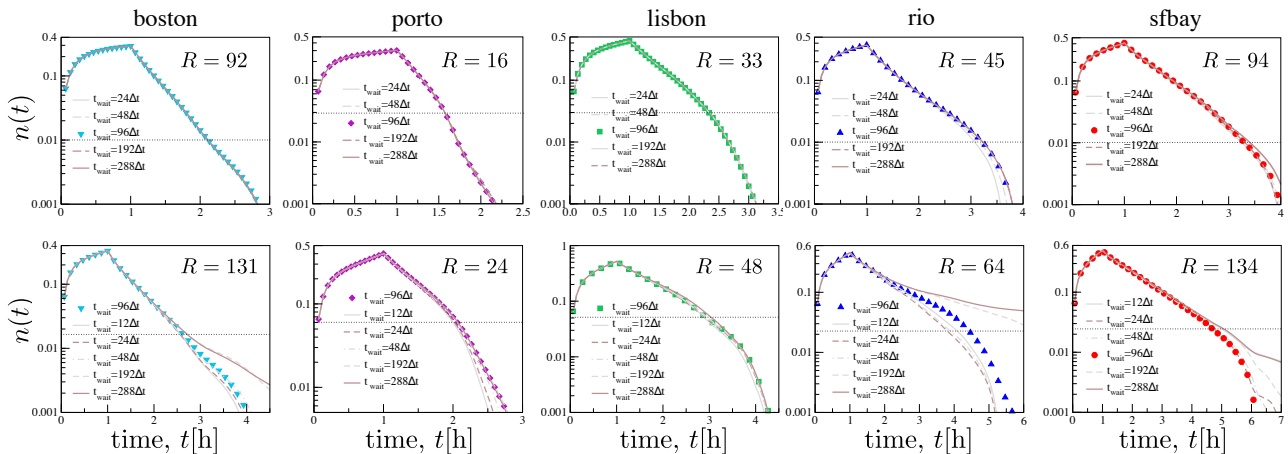


**Fig. S9.** Sensitivity Analysis of  $\tau$  to the parameter  $t_{wait}$ . It is worth remembering the re-routing strategy: A vehicle that has been stopped at an intersection during more than  $t_{wait}$  time steps, reroutes to a less congested destination street and recomputes its route. It should be noted in passing that if the vehicle behind has the same destination street (as expected in the arteries), it will wait  $t_{wait}$  time steps before decides to reroute. Thus, in a queue, the waiting time grows arithmetically with the number of cars in the street. If  $t_{wait}$  is too small, vehicles would change their routes unnecessarily, especially under low traffic conditions. In contrary, if  $t_{wait}$  is too large, it could generate artificial gridlocks in the network. We have chosen  $t_{wait}=96$  time steps ( $\approx 2$  minutes) as an intermediate value. Curves on the top correspond to the current traffic conditions ( $R_{ca}$ ). The horizontal lines denote the cut-off to measure  $\tau$ , i.e. when  $n(t)$  reaches a value ranging from 1% to 4%. Under current conditions,  $\tau_{ca}$  is insensitive to the parameter  $t_{wait}$ . For higher demand levels, panels in the bottom,  $t_{wait}$  become important. For Rio de Janeiro, in particular, the exponential decay distorts for  $t_{wait} > 96$  time steps. However,  $\tau$  varies slightly for  $t_{wait} \leq 96$ .

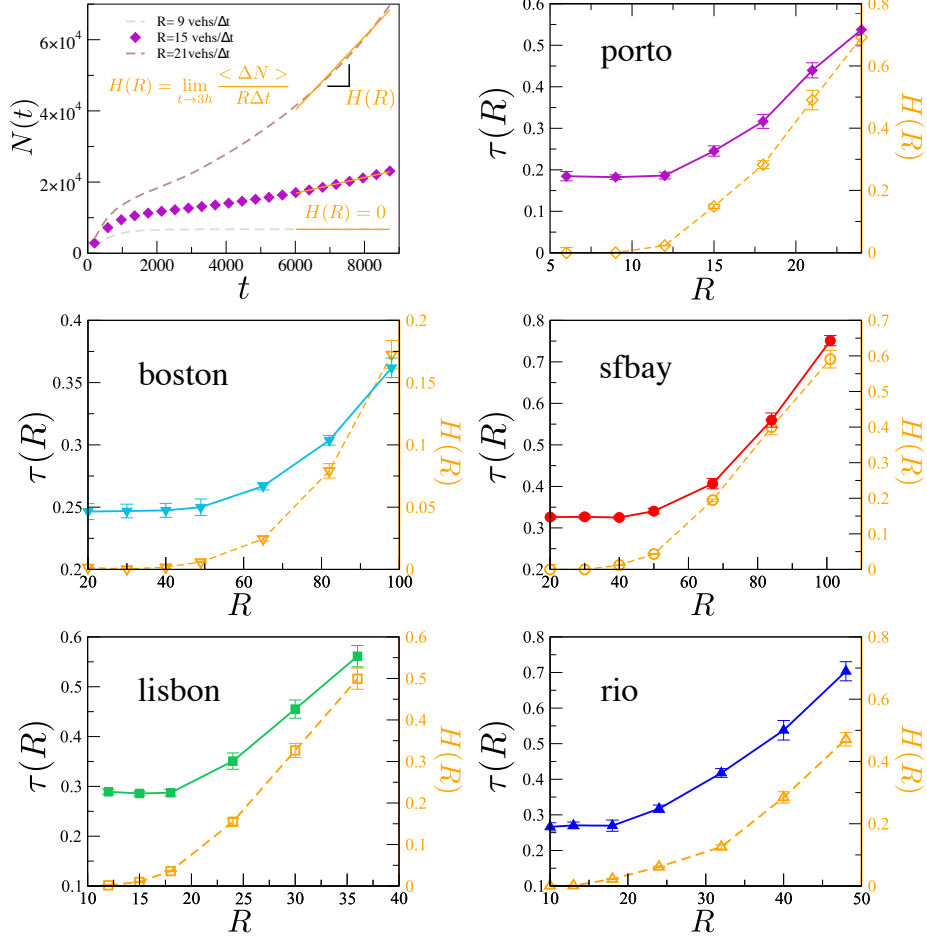


**Fig. S10.** The meaning of  $\Gamma_1^i$ . The scheme used to study traffic and congestion phenomena on complex networks is as follows(5): the network is loaded with  $R$  identical particles (vehicles) at each time step  $\Delta t$  with, in general, randomly assigned origins and destinations. These particles travel to their destination following a certain routing dynamics and then removed from the system upon arrival. The nodes can transmit as many particles per time step as their capacity,  $C_{node}$ , and particle travel from one node to another in a unit time step. Queues of particles form at the nodes, and they can grow infinitely. The total network load or traffic is determined by the number of particles traveling simultaneously on the network. The network response is measured by the order parameter  $H$ ,  $H(R) = \lim_{t \rightarrow T} \frac{\langle \Delta N \rangle}{R \Delta t}$ , where  $N$  denotes the number of particles in the system,  $\langle \Delta N \rangle$  is the average change in the number of particles still in the network after a times step,  $\Delta t$ , and  $T$  is the length of the simulation. For low values of  $R$ , the load ( $N$ ) fluctuates around a steady-state value, meaning that the insertion rate equals the trip completion rate, and thus  $H=0$ . Conversely, if  $R$  exceeds a certain threshold  $R_c$ , due to the queuing process,  $N$  increases linearly with a slope  $H(R)$ . Top-left figure depicts this behavior using constant insertion rates on Porto. Trips are randomly chosen from the empirical ODs and the traffic dynamics is modeled with the proposed cellular automaton model. The other figures show the behavior of  $H(R)$  (in a constant loading framework) and  $\tau(R)$  (in our 1h loading framework) for the simulated cities. We can observe how both  $\tau(R)$  and  $H(R)$  start to increase at the vicinity of the same  $R_c^i$ , corresponding to a specific  $\Gamma_1^i$ .

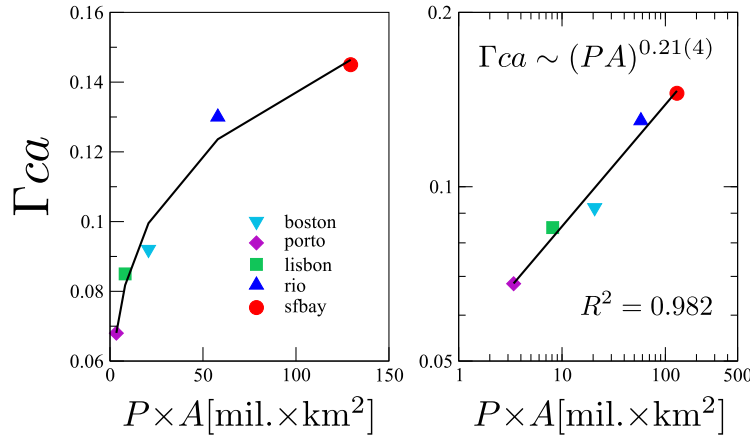


**Fig. S11.**  $\Gamma_{ca}$  as a function of city size In agreement with recent studies(6–9), we found an allometric scaling between  $\Gamma_{ca}$  and city population ( $P$ ) and area ( $A$ ).

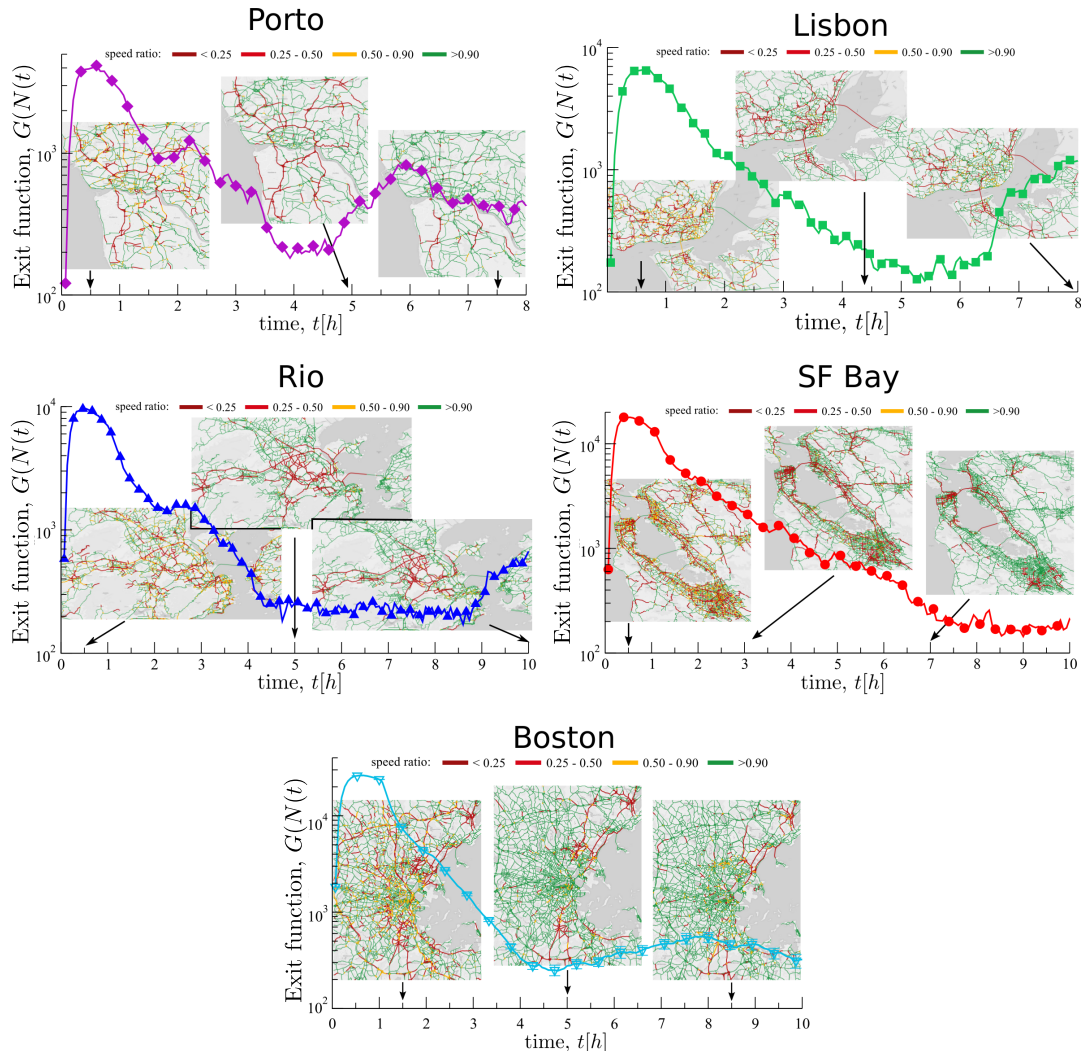


**Fig. S12. Snapshots of the urban traffic at three different times of its evolution under a very high traffic demand, i.e.  $R > R_c$  in each case. We consider the normalized speed on every link, defined as the vehicles speed (with 4-minutes resolution) divided by the speed limit in that link. Thus, the road segments are classified into three categories according to the speed ratio: below 0.5 (red), between 0.4-0.9 (yellow) and above 0.9 (green). The clusters of in red depict long-lasting traffic jams.**

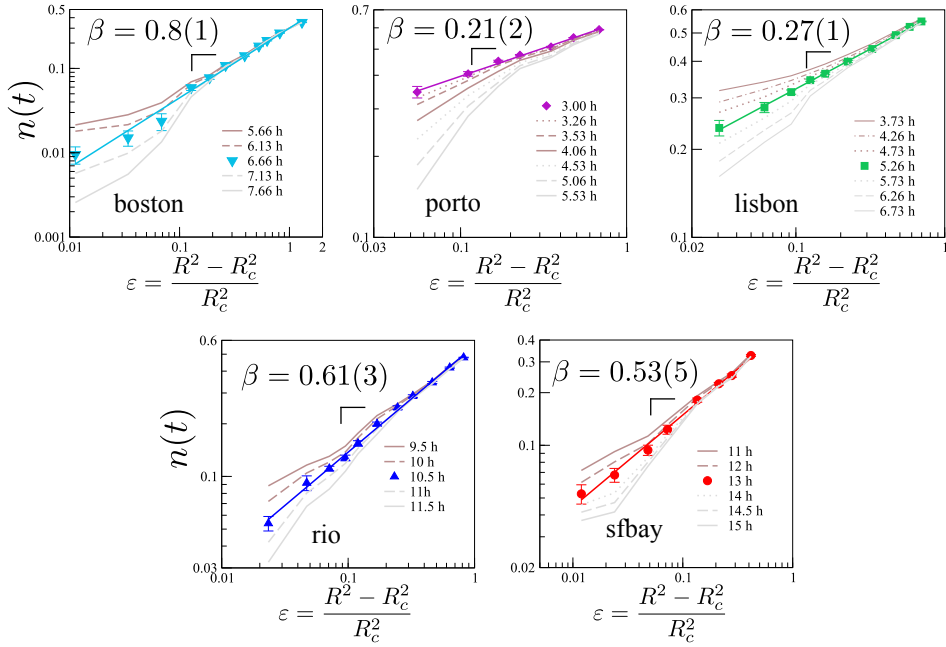


**Fig. S13.** Definition of the order parameter  $N(R)$ . We define  $n(R)$  as the remaining percentage of vehicles in the network at the collapsed state. Figure shows  $n(R)$  for the times,  $t$ , depicted in the legends. To measure  $n(R)$ , we set  $t$  as the moment at which the better fit  $n(R) \sim \varepsilon^\beta$  is obtained, colored symbols for each city.

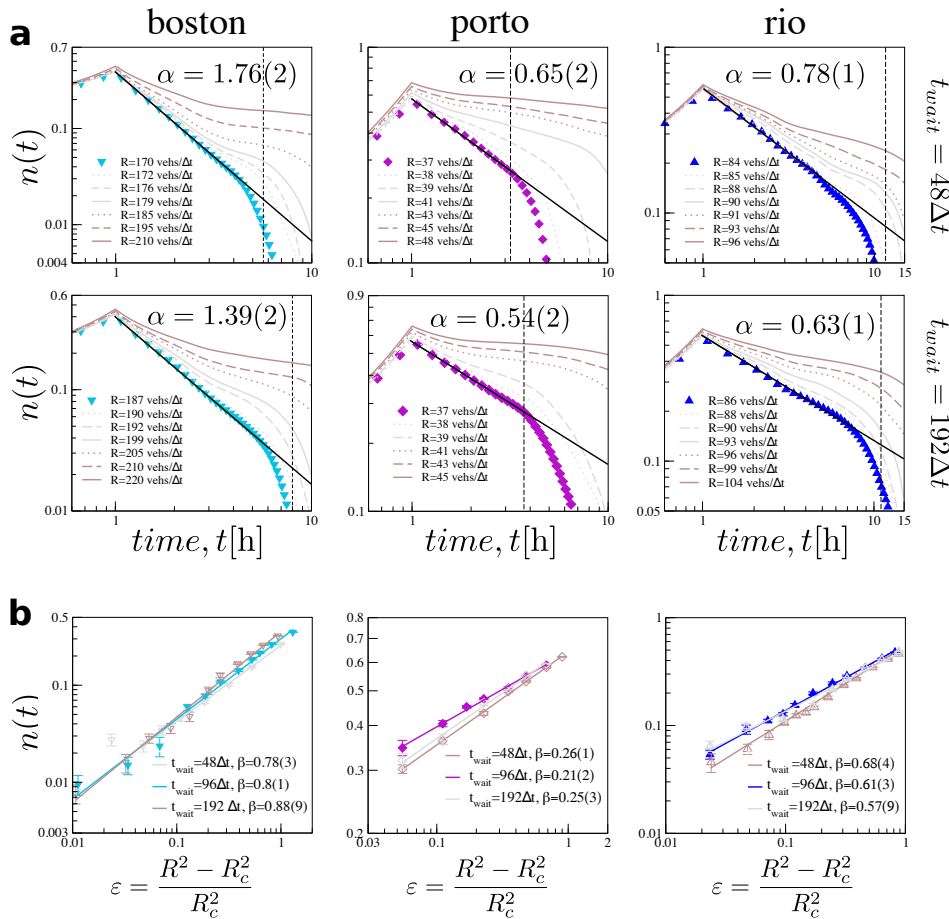


**Fig. S14.** Sensitivity analysis of the critical properties to the parameter  $t_{wait}$ . (a) Temporal dynamics of  $n(t)$  under different travel demands. We determine  $\alpha$  and  $R_c$  for each  $t_{wait}$ . (b) Measurements of  $\beta$ , which seems to be robust with the value of the parameter  $t_{wait}$ .

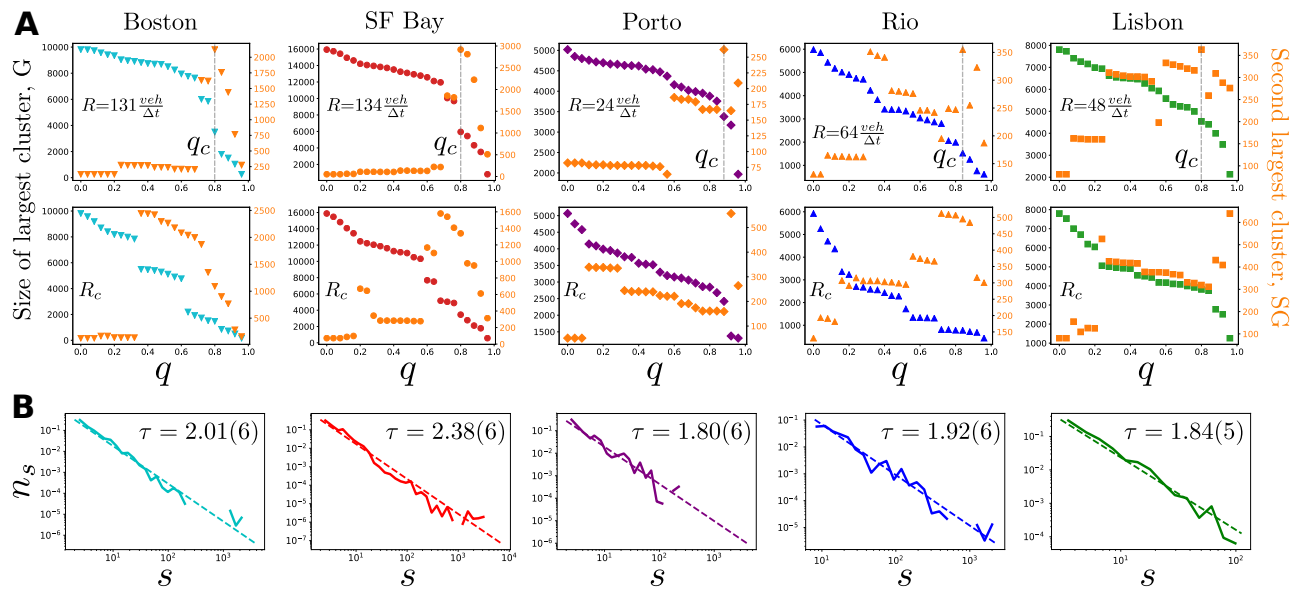


**Fig. S15. Percolation-like processes in city traffic around the morning peak hour (8:30 am).** Using the same framework in (10), for each road segment  $e$  we measure the ratio between its current velocity ( $v_e(t)$ ) and its maximal velocity ( $v_e^m$ , measured at free flow conditions). According to this ratio, each road segment is classified into two categories: functional (If  $(v_e(t))/(v_e^m) > q$  road stays within the network) and dysfunctional ( $(v_e(t))/(v_e^m) < q$ , road is removed). A percolation-like transition can be observed by tracking the size of the largest functional cluster,  $G$ . As  $q$  increases, the size of  $G$  decreases and the second-largest cluster  $SG$  reaches a maximum at the critical threshold  $q_c$  separating the fragmented phase from the connected phase of the traffic network. As hundreds of roads are not highly used, we have only considered motorways in this specific analysis and velocity ratios are averaged over 10 minutes. (A) Size of the largest cluster  $G$  (colored symbols) and the second-largest cluster  $SG$  (orange symbols) of traffic networks as a function of  $q$ . For a travel demand within the traffic jams region (Top), Boston and San Francisco are in consonance with the above description, we observe a  $q_c \approx 0.8$  for both cities. For the other cities the behavior is a little more complex, the fragmentation of  $G$  is progressive over a wide  $q$  range, and there is not a clear critical point,  $q_c$ , at which  $SG$  becomes large. Thus, instead of a global traffic, city traffic decomposes into several clusters of local flows separated by many bottlenecks scattered throughout the city. Similar results are observed for travel demands in the vicinity of the collapse of the network  $R_c$  (bottom same figure). Interestingly, multiple abrupt fragmentations can be observed in the cases of Boston and San Francisco. For a future work, the question that arises is to what extent these results depend on the simple CA model used for the vehicular dynamics. Under the same percolation framework, the size distribution of clusters has been studied in (11). They have shown that close to  $q_c$ , the size distribution of finite clusters follows a power law  $n_s \sim s^{-\tau}$ . They have found that the critical exponent  $\tau$  is close to the result of two-dimensional lattice percolation ( $\approx 2.0$ ) during rush hours in workdays while close to small-world during other periods ( $\approx 2.5$ ). The authors argue that a key point affecting the value of  $\tau$  is the fraction of the effective long range connections represented by the free highways. We have performed a similar analysis in our cities with the travel demand conditions in A (top) at peak hour 8:30 am. Here  $q_c$  is pragmatically defined as the point at which  $SG$  reaches a maximum. (B) Cluster size distribution after logarithmic binning, used to calculate the critical exponent  $\tau$ . Our  $\tau$  values range from 1.80 to 2.38.

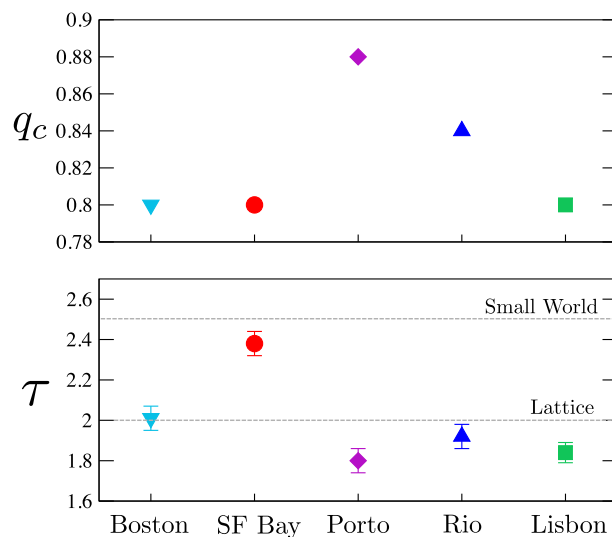


**Fig. S16. Critical threshold  $q_c$  and critical exponent  $\tau$  obtained for each city.** The values of  $\tau$  are consistent to the values reported in (11). In contrast, we find higher values of  $q_c$  in our simulations.

**A. Effects of congestion pricing and routing policies from the perspective of our work:** Our findings rely mainly on the exponential decongestion observed in empirical data. We have shown this feature is a consequence of the log-normal distribution of travel distances (Fig. S5), and thus we expect thus a congestion pricing policy should not affect this decongestion feature, and thus the general description of our findings will remain unchanged; these strategies would change the volume over capacity in certain links, decreasing  $\Gamma$  and in consequence the  $\tau$ , of the demand.

Overall, leaving equity issues aside, routing(12) and congestion pricing schemes(13–15) reduce successfully the travel times mainly by two reasons: (1) deters the personal use cars (as in road an cordon pricing) or (2) encourages drivers to divert their paths to neighboring and less congested regions. Interestingly, we can expect the same results from the perspective of our work. Reason (1) becomes in a reduction in the vehicle-miles traveled (VMT), which is the numerator of  $\Gamma^i$ . Reason (2) suggests a better trips distribution, increasing the use of the infrastructure, i.e. the denominator of  $\Gamma^i$ . Thus, under the current traffic conditions, any congestion pricing scheme will reduce the demand to supply  $\Gamma^i$  and thus the unloading travel time  $\tau^i$ .

However, since a hotspot pricing and routing schemes can produce a great change in the distribution of trips, much stronger than the rerouting strategies, we should expect crucial changes for the critical situations. We explain why: Note that the transition thresholds  $\Gamma^i$  (first bottleneck emerges) and  $R_c$  (collapse of the network) are entirely related with the betweenness centrality  $B_k$  of the node (or road segment). That is to say, the first bottlenecks appear at the nodes (road segments) with highest betweenness centrality  $B_k$ , and those first failures are usually the focus around which the gridlocks appear and grow, thus driving to the network collapse. Any strategy that incentivizes the better distribution of trips will delay the failures and thus increase the values of  $\Gamma^i$  and  $R_c$ , implying small changes in the slopes in Fig. 3 in the manuscript, and thus maintaining the scaling obtained. In the same reasoning line, a better distribution of traffic will produce more hotspots with a lower level of failure, thus we can expect a more resilient traffic network and an increase in the critical exponents (Fig. 5B in the manuscript).

1. Mazloumian A, Geroliminis N, Helbing D (2010) The spatial variability of vehicle densities as determinant of urban network capacity. *Phil. Trans. R. Soc. A* 368:4627–4647.
2. Daganzo CF, Gayah VV, Gonzales EJ (2011) Macroscopic relations of urban traffic variables: Bifurcations, multivaluedness and instability. *Transportation Research B* 45(1):278–288.
3. Herman R, Prigogine I (1979) A two-fluid approach to town traffic. *Science* 204:148–151.
4. Mahmassani H, Williams J, Herman R (1984) Investigation of network-level traffic flow relationships: some simulation results. *Transportation Research Record: Journal of the Transportation Research Board* 971:121–130.
5. Barrat A, Barthélémy M, Vespignani A (2012) *Dynamical Processes o Complex Networks*. (Cambridge University Press).
6. Samaniego H, Moseley ME (2008) Cities as organisms: Allometric scaling of urban road networks. *Journal of Transport and Land Use* 1:21–39.
7. Bettencourt LMA (2013) The origins of scaling in cities. *Science* 340:1438.
8. Louf R, Barthelemy M (2014) How congestion shapes cities: from mobility patterns to scaling. *Scientific Reports* 4:5561.
9. Bettencourt LM, Lobo J, Helbing, D, KC, West GB (2007) Growth, innovation, scaling, and the pace of life in cities. *Proc. Natl Acad. Sci. (USA)* 104:7301–7306.
10. Li D, et al. (2015) Percolation transition in dynamical traffic network with evolving critical bottlenecks. *Proc. Natl. Acad. Sci.* 112(3):669–672.
11. Zeng G, Li D, Gao L, Gao Z, Havlin S (2017) Switch of critical percolation modes in dynamical city traffic. arxiv:1709.03134. *Preprint posted 10 September 2017*.
12. Zhang J, Pourazarm S, Cassandras CG, Paschalidis IC (2018) The price of anarchy in transportation networks: Data-driven evaluation and reduction strategies. *Proceedings of the IEEE* 106(4).
13. Mun Si, Konishi Kj, Yoshikawa K (2003) Optimal cordon pricing. *Journal of Urban Economics* 54:21–38.
14. Kraus M (1989) The welfare gains from pricing road congestion using automatic vehicle identification and on vehicle meters. *Journal of Urban Economics* 25:261–281.
15. Solé-Ribalta A, Gómez S, Arenas A (2017) Decongestion of urban areas with hotspot pricing. *Netw. Spat. Econ.* pp. 1–18.